INTERNATIONAL JOURNAL FOR NUMERICAL METHODS IN FLUIDS, VOL. 10, 697–711 (1990)

A FINITE DIFFERENCE SELF-ADAPTIVE MESH SOLUTION OF FLOW IN A SEDIMENTATION TANK

MARCO CASONATO AND FRANCESCO GALLERANO

Dipartimento di Idraulica, Trasporti e Strade, Università degli Studi di Roma 'La Sapienza', Rome, Italy

SUMMARY

A new numerical model has been developed to evaluate the removal efficiency of primary sedimentation clarifiers operating at neutral density condition. The velocity and concentration fields as well as the development in time and space of the settled particle bed thickness are simulated. The main difficulties in simulation of velocity and concentration fields are related to (1) numerical instabilities produced by the prevalence of convective terms in the unknown variable high-gradient regions and (2) turbulence effects on the suspension of solid particles from the settled bed. The need to overcome the numerical instabilities without the upwind difference approximation, which introduces high numerical viscosity, suggests the use of non-uniform grids of calculation.

The velocity field is obtained by solving the motion equations in the vorticity and streamfunction formulation by means of a new numerical method based upon a dynamically self-adjusting calculation grid. These grids allow for a finer mesh following the evolution of the unknown quantities. A k–ε model is used to simulate turbulence phenomena.

The sedimentation field is found by solving the diffusion and transport equation of the solid particle concentration. Boundary conditions on the bottom line are imposed relating the amount of turbulence flux and sedimentation flux to the actual concentration and the reference concentration. Such an approach makes it possible to represent the solid particle suspension from the bottom, taking into account its dependence on (1) the characteristics and the evolution in time of the settled bed, (2) the velocity component parallel to the bottom line and (3) the turbulence structure.

KEY WORDS Sedimentation tank Adaptive calculation grid Vorticity and streamfunction Particle concentration k–ε model Numerical instabilities L.D.A. test

INTRODUCTION

Analysis of the settling performance of primary clarifiers requires detailed knowledge of the velocity field in the tanks. Since the flow is turbulent and recirculating flow patterns are present in the basin, the velocity field is difficult to simulate. Furthermore, the sedimentation phenomenon is complex, since there is an interacting two-phase turbulent flow in which effects may induce density differences within the tank and therefore cause modifications of the flow pattern.

The possibility of simulating the liquid phase uncoupled from its solid phase counterpart is presently being debated. In fact, Hudgins and Silveston[1] have disputed the Imam and McCorquodale hypothesis[2] of uncoupling the phases, because in this case the stratified flows produced by concentration gradients are neglected. McCorquodale's answer[3] is convincing with regard to the reduced presence of flow field modifications produced by the solid phase in primary sedimentation, and emphasizes the importance of small temperature differences between inflow and outflow in producing density currents as well as in modifying the turbulent structures. Schamber and Larock[4] state that if the particle suspension is sufficiently dilute then the

0271–2091/90/060697–15$07.50

Received February 1989
Revised July 1989

simulation of the hydrodynamics may be done separately from the simulation of particle transport, while Di Giacinto *et al.*[5] show that the Froude number together with the ratio between the volume fraction of the two phases and the ratio between the microscopic density of the two phases are the parameters which indicate the conditions of uncoupling.

Thus in the absence of temperature gradients and in the case of dilute suspensions the velocity field can be analysed alone: consequently the removal efficiency of the sedimentation basin depends on the turbulent mixing and on the vertical and horizontal recirculation flow patterns. The cost of three-dimensional computation is currently prohibitive in terms of computer time and storage, thus we have to restrict the analysis of the flow to a vertical plane taken on the tank centreline from inlet to outlet. Schamber and Larock[6] consider this approach reasonable in the absence of wind stresses.

Good simulations of turbulent structures require the use of at least two equation models.[7] Simpler turbulent models do not provide reliable results. However, the suggestion of Imam and McCorquodale[2] is of interest, which simulates the flow field in primary sedimentation tanks by solving, using finite differences, the Navier–Stokes equations in terms of vorticity and streamfunctions; the use of alternate direction implicit techniques is suitable and the instability induced by the dominance of the advective terms is avoided by means of the upwind formulation, while the eddy viscosity coefficient is assumed to be constant. Abdel-Gawad and McCorquodale[8] use an original method based on a combination of strip integral and finite element methods to simulate the flow field in rectangular sedimentation tanks; a modified mixing length approach is used to introduce the effect of turbulence in the solution.

The use of more sophisticated turbulent models provides more satisfactory solutions, but such models present problems of stability and convergence of the algorithm. These instabilities, as well as those arising where the convective terms are prevalent can be overcome by a selective refinement of the mesh in high-gradient regions. Schamber and Larock[6] solve the problem in an interesting way: the flow field is obtained by a finite element solution of five partial differential equations in terms of mean vertical and horizontal velocity, mean pressure, kinetic energy of turbulence and viscous dissipation. The finite element method allows for the use of a non-uniform computation mesh in the space.

Generally the simulation of the sedimentation field is obtained by numerically solving the diffusion and transport equation of the suspended solid concentration. Such an equation needs suitable boundary conditions. The definition of boundary conditions at the bottom of the tank, where the bed of settled particles is located, is particularly complex and essentially related to (1) the characteristics of the settled particles, (2) the shear stress which produces the movement of the bed particles and (3) the turbulence structure which causes the upward movement of the particles.

Schamber and Larock[4] set the boundary condition at the bottom by assuming that the upward flux due to turbulence is equal to a fraction of the downward flux due to sedimentation. The time changes and the variations in turbulence and in velocity along the bottom line are not taken into account; the same treatment is given to the changes in sedimentation velocity, which is a function of the concentration. It is clear that the previous approach makes it possible to define the removal efficiency curve as a function of the sedimentation velocity, having defined *a priori* the suspension coefficient and taking it as being constant in time and space.

The possibility of numerically predicting concentration fields and removal efficiencies is then excessively dependent on experimental measurements, which are necessary to define the bottom suspension coefficient for each case.

The development of models that give valid design indications and that are not subordinated to information deriving from experimental measurement, requires the definition of methodologies

able to determine, in an inexpensive way in terms of computing time, the structure of the bottom suspension as a function of all the parameters involved in the phenomenon.

This paper presents a numerical model for the simulation of velocity and concentration fields as well as the time evolution and the thickness trends of the settled bed along the bottom line. The velocity field is obtained by solving the Reynolds equation in the vorticity and streamfunction formulation, using a new numerical method based on a self-adaptive mesh following the evolution of the problem's unknown quantities. A k–ε model is used to simulate the turbulent phenomena. The sedimentation field is determined by solving the diffusion and transport equation of the concentration. The boundary conditions at the bottom line of the tank are set by relating the amount of turbulence flux and sedimentation flux to the actual concentration and the reference concentration, which are variable in time and space, being functions of the characteristics of the velocity component parallel to the bottom.

MATHEMATICAL MODEL

Velocity field

The equations describing a two-dimensional, unsteady, turbulent, non-stratified flow in a rectangular sedimentation basin are

$$\frac{\partial u}{\partial x} + \frac{\partial v}{\partial y} = 0, \tag{1}$$

$$\frac{\partial u}{\partial t} + u\frac{\partial u}{\partial x} + v\frac{\partial u}{\partial y} = -\frac{1}{\rho}\frac{\partial p}{\partial x} + \nu\left(\frac{\partial^2 u}{\partial x^2} + \frac{\partial^2 u}{\partial y^2}\right) - \left[\frac{\partial \overline{u'^2}}{\partial x} + \frac{\partial(\overline{u'v'})}{\partial y}\right], \tag{2}$$

$$\frac{\partial v}{\partial t} + u\frac{\partial v}{\partial x} + v\frac{\partial v}{\partial y} = -\frac{1}{\rho}\frac{\partial p}{\partial x} + \nu\left(\frac{\partial^2 v}{\partial x^2} + \frac{\partial^2 v}{\partial y^2}\right) - \left[\frac{\partial \overline{v'^2}}{\partial y} + \frac{\partial(\overline{u'v'})}{\partial x}\right], \tag{3}$$

in which u and v are the horizontal and vertical components of mean velocities, u' and v' are the instantaneous velocity fluctuations around their respective means, ρ is the fluid density, ν is the kinematic viscosity and p is the pressure.

Using the relationships

$$\frac{\partial \psi}{\partial y} = u, \qquad \frac{\partial \psi}{\partial x} = -v, \qquad \omega = \frac{\partial u}{\partial y} - \frac{\partial v}{\partial x}, \tag{4}$$

in which ψ is the streamfunction and ω is the vorticity, equations (1)–(3) can be replaced in the following way:

$$\frac{\partial \omega}{\partial t} + u\frac{\partial \omega}{\partial x} + v\frac{\partial \omega}{\partial y} = \frac{1}{Re}\nabla^2 \omega - \frac{\partial}{\partial x}(\overline{u'\omega'}) - \frac{\partial}{\partial y}(\overline{v'\omega'}), \tag{5}$$

$$\nabla^2 \psi = \omega, \tag{6}$$

in which $Re = U_0 L_0/\nu$, where U_0 and L_0 are characteristic velocity and length scales.

With the assumption that the vorticity ω is a 'transferable quantity' (Taylor's vorticity–transport theory), the correlations for the turbulence fluctuation of velocity and vorticity can be related to the gradient of the average vorticity by

$$\overline{u'\omega'} = \nu_T \frac{\partial \omega}{\partial x}, \qquad \overline{v'\omega'} = \nu_T \frac{\partial \omega}{\partial y}. \tag{7}$$

The eddy viscosity coefficient ν_T assumes the same value of the proportionality coefficient between correlations for turbulence fluctuation of velocity and the mean velocity derivative. This assumption is strictly demonstrable only for uniform bidimensional flow.[9]

The eddy viscosity coefficient is related to the turbulent kinetic energy k and its rate of dissipation ε by

$$\nu_T = c_\mu k^2/\varepsilon, \tag{8}$$

in which c_μ is a constant equal to 0·09.[7]

The variables k and ε are computed from the transport partial differential equations coupled with the streamfunction and vorticity equations to obtain the simulation of the turbulent flow field.

Assuming that P, the turbulent kinetic energy production, is given by

$$P = \nu_T\left[2\left(\frac{\partial u}{\partial x}\right)^2 + 2\left(\frac{\partial v}{\partial y}\right)^2 + \left(\frac{\partial u}{\partial y} + \frac{\partial v}{\partial x}\right)^2\right], \tag{9}$$

the k–ε equations have the form

$$\frac{\partial k}{\partial t} + u\frac{\partial k}{\partial x} + v\frac{\partial k}{\partial y} = P + \frac{\partial}{\partial x}\left(\frac{\nu_T}{\sigma_k}\frac{\partial k}{\partial x}\right) + \frac{\partial}{\partial y}\left(\frac{\nu_T}{\sigma_k}\frac{\partial k}{\partial y}\right) - \varepsilon, \tag{10}$$

$$\frac{\partial \varepsilon}{\partial t} + u\frac{\partial \varepsilon}{\partial x} + v\frac{\partial \varepsilon}{\partial y} = c_{\varepsilon_1}\frac{\varepsilon}{k}P - c_{\varepsilon_2}\frac{\varepsilon^2}{k} + \frac{\partial}{\partial x}\left(\frac{\nu_T}{\sigma_\varepsilon}\frac{\partial \varepsilon}{\partial x}\right) + \frac{\partial}{\partial x}\left(\frac{\nu_T}{\sigma_\varepsilon}\frac{\partial \varepsilon}{\partial y}\right), \tag{11}$$

in which the constants c_{ε_1}, c_{ε_2}, σ_k and σ_ε have the values 1·44, 1·92, 1·0 and 1·3 respectively.

Since the k–ε model is adopted to simulate the structures of turbulence, one does not require *a priori* knowledge of the distribution of ν_T, but the complexity of computation is increased. On the other hand, use of turbulent models in which no additional differential equations are required for turbulence closure does not provide reliable results. In fact, in these cases, it is difficult to obtain a turbulent flow field in which the main eddy characteristics are in agreement with experimental measurements; in particular, it is difficult to compute a correct value of both the reattachment point and the centre of the main eddy.

Equation (6)–(11) represent a closed system of equations relating vorticity, streamfunction, kinetic energy of turbulence and its dissipation rate. Boundary conditions are required to yield a unique solution.

Figure 1 shows the solution domain for a rectangular clarifier.

A parabolic profile of the horizontal component of velocity is imposed along the inlet line A–B; the streamfunction ψ_0 along this line has a cubic profile and the vorticity is given by

$$w = \frac{\partial^2 \psi}{\partial x^2} + \frac{\partial^2 \psi_0}{\partial y^2}. \tag{12}$$

The values of k and ε are also imposed along A–B in agreement with Rodi's suggestion.[7] The lines B–C, C–D, D–E, represent rigid walls where the components of the velocity and streamfunctions normal to the wall are assumed equal to zero and the vorticity is given by

$$w = \frac{\partial^2 \psi}{\partial x^2} \quad \text{on vertical walls,} \qquad w = \frac{\partial^2 \psi}{\partial y^2} \quad \text{on the bottom.} \tag{13}$$

With regard to the boundary conditions on k and ε along these planes, it should be noted that the turbulent model is valid only in fully turbulent flow; Launder and Spalding's suggestions[10]

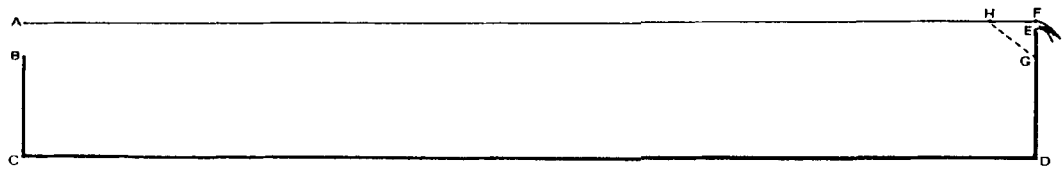

Figure 1. Solution domain for a rectangular clarifier

and the applications to sedimentation basins carried out by Schamber and Larock[6] indicate a way to solve this problem: k and ε are not assigned at the wall but at a distance y^* from the wall, where there is a fully turbulent regime. In this region, convection and diffusion of $\overline{u'v'}$ are negligible; thus in the absence of buoyancy effects, the turbulent kinetic energy production is equal to the dissipation rate. Boundary conditions on k and ε become

$$k=\frac{U_\tau^2}{\sqrt{c_\mu}}, \qquad \varepsilon=\frac{U_\tau^3}{\chi y^*}, \tag{14}$$

in which U_τ is the friction velocity given by

$$\frac{U_r}{U_\tau}=\frac{1}{\chi}\ln\left(\frac{y^* U_\tau}{\nu}E\right), \tag{15}$$

where U_r is the velocity component parallel to the wall, E is a roughness parameter (which was given a value of 9)[7] and χ is the von Karman constant.

The line A–F represents the free surface where the vertical component of velocity and the vorticity are set equal to zero, the streamfunction is constant and equal to Q (flow rate) and the conditions $\partial\omega/\partial y=0$, $\partial k/\partial y=0$, $\partial\varepsilon/\partial y=0$ are assumed. The line E–F represents the outflow. This line is shorter than a computational grid step. The boundary conditions on ω and ψ are not difficult to impose (in agreement with Imam and McCorquodale's suggestions[2]). With regard to the boundary conditions on k–ε at the outflow, since experimental data are not available and to avoid excessive thickening of the mesh in this region, the boundary is assumed to be the line G–H; as suggested by Schamber and Larock,[6] the normal derivatives of k and ε along it are set equal to zero.

Concentration field

The sedimentation field is determined by solving the equation of the concentration diffusion and transport:

$$\frac{\partial c}{\partial t}+u\frac{\partial c}{\partial x}+(v-v_s)\frac{\partial c}{\partial y}=\frac{\partial}{\partial x}\left[\frac{\nu_T}{\sigma_T}\left(\frac{\partial c}{\partial x}\right)\right]+\frac{\partial}{\partial y}\left[\frac{\nu_T}{\sigma_T}\left(\frac{\partial c}{\partial y}\right)\right], \tag{16}$$

where c is the concentration, v_s is the sedimentation velocity and σ_T is Schmidt's number.

At the inlet, boundary conditions are expressed by assigned values of the concentration. At the free surface and at vertical walls the net flux of particles is set equal to zero, namely

$$v_s c+\frac{\nu_T}{\sigma_T}\frac{\partial c}{\partial y}=0 \quad \text{at the free surface,} \tag{17}$$

$$\frac{\partial c}{\partial x}=0 \quad \text{at vertical walls.} \tag{18}$$

At the inlet, namely along the line G–H of Figure 1, advective transport is more important than diffusion transport; thus the derivative of the concentration respect to the normal to line G–H is set equal to zero.

At the bottom, boundary conditions are present (from the definition of the reference concentration as suggested by Armanini and Di Silvio[11]).

Such a reference concentration c_{ar} is the concentration at a distance a from the bed of sedimented particles in equilibrium conditions, namely in the absence of sedimentation or suspension. The net particle flux, i.e. normal to the line located at a distance a from the bed, is given by the product of the sedimentation velocity and the difference between the actual concentration and the reference concentration. Thus the boundary conditions for the bottom become

$$\frac{v_T}{\sigma_T}\frac{\partial c}{\partial y} = c_k v_s c, \tag{19}$$

where c_k is the suspension coefficient given by

$$c_k = c_{ar}/c. \tag{20}$$

Such a coefficient is variable along the bottom line and in time with respect to the actual and the reference concentration.

The reference concentration is usually difficult to estimate. In this analysis the hypothesis formulated by van Rijn[12] is assumed:

$$c_{ar} = 0{\cdot}015\frac{d}{a}\frac{T_*^{1{\cdot}5}}{D_*^{0{\cdot}3}}, \tag{21}$$

in which

$$D_* = d\left(\frac{(s-1)g}{v}\right)^{1/3}, \qquad T_* = \frac{U_r^2 - u_{cr}^2}{u_{cr}^2}, \tag{22}$$

where d is the particle diameter, s is the specific density, v is the cinematic viscosity coefficient and u_{cr} is the critical bed-shear velocity.

The critical bed-shear velocity is given by

$$u_{cr} = 0{\cdot}25\, v_s. \tag{23}$$

The change in time of the bed thickness z is

$$\frac{\partial z}{\partial t} = v_s(c - c_{ar}). \tag{24}$$

CALCULATION PROCEDURE AND SELF-ADAPTIVE MESH GENERATION

The calculation method used to solve the system of equations is based on the finite difference technique. The particular geometry of the sedimentation tank, which is marked by greater length than depth, suggests the use of a variable and self-adaptive grid in order to obtain greater computational stability and more accurate results. A self-adaptive grid also makes it possible to describe the flow field better when higher gradients of the unknown functions arise; this situation is present especially in the inlet and outlet zones.

Furthermore, in these regions computational instabilities or wiggles at the centre of the convective terms can arise during the finite difference approximation. Generally, these in-

stabilities are overcome by an upwind difference scheme, which, however, has the disadvantage of introducing additional numerical diffusion. Numerical experiments[13] have shown that a finer mesh in high-gradient regions reduces instabilities in a centred difference scheme and reduces numerical diffusion produced by upwind schemes. On the other hand, the possibility of thickening the mesh where convective terms are higher is limited by the need to have a time integration step sufficiently large to avoid heavy computational costs. The most common finite difference methods non-uniform grids are based on a co-ordinate transformation from the physical domain to the calculation domain: the differential equations to be solved are first rewritten in the transformed plane and then approximated by a finite difference scheme. These methods have the following disadvantages.

(1) The problem of automation of grid generation to follow the evolution of the unknown quantities is solved by obtaining the co-ordinate transformation through numerical solution of some elliptic partial differential equations.
(2) Thickening of the mesh in one region is accompanied by a depletion in adjacent regions, so it is not possible to modify a small part of the grid during the calculation without moving a major portion of all points.

The approach followed in this paper to obtain the self-adapting mesh without co-ordiante transformation is based on the observation that the finite difference approximation of the Laplacian operator written on five points of a symmetrical cross is very accurate and simple, whereas, if the symmetry is broken, much accuracy is lost. Consequently a local thickening can be obtained, without any change in the remaining computational domain, by introducing a new point among four existing points: thus a new symmetrical cross is generated which is inclined at 45° with respect to the pre-existing crosses and has shorter branches. In this way a scheme of creation and deletion of points is adopted which allows for (dynamically self-adjusting) selective mesh refinement in high-gradient regions, which is simpler than the finite element method refinement and does not have the disadvantages produced by finite difference methods based on co-ordinate transformation. For further explanation, compare Figure 2(a) with Figure 2(b). In Figure 2(a), point 5 is the point at the centre of the symmetric cross having the points 8, 2, 6, 4 as its extremes. In Figure 2(b), five points and relative symmetrical crosses have been introduced: point 10, which is at the centre of the cross with points 5, 1, 2, 4 as its extremes; point 11 and the cross with 6, 2, 3, 5 as extreme points; point 12 and the cross with 8, 4, 5, 7 as extreme points; point 13 and the cross with 3, 5, 6, 8 as extreme points; point 14 with 8, 5, 13, 12 as extreme points. Consequently, point 5 is the centre of a new cross which is inclined and smaller than the pre-existing cross. Of course the adaptive mesh process can also remove the extra mesh points when they are no longer needed.

The calculation procedure to integrate equations (5), (6), (10), (11) and (16) consists of a time iteration which starts from an initial condition and reaches the steady solution.

Assume that:

N^t number of points located within the boundary lines at iteration t
N_B^t number of points on boundary lines at iteration t.

We define the following vectors:

$\boldsymbol{\omega}^t$ whose dimension is N^t; ω_i^t represents the value of the vorticity at point i at iteration t
$\boldsymbol{\psi}^t$ whose dimension is N^t; ψ_i^t represents the streamfunction at point i at iteration t
$\mathbf{H}^t$ whose dimension is N^t; H_i^t represents the branch length of the symmetrical cross with the point i as its central point

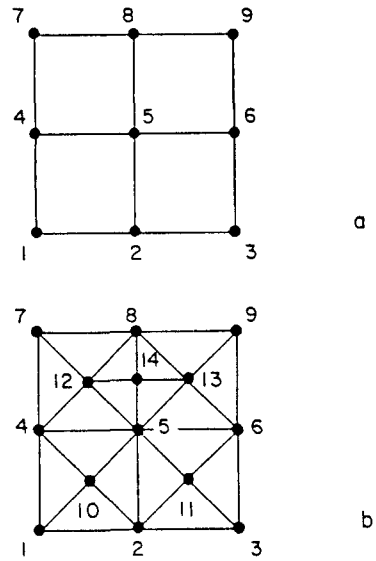

Figure 2. (a) Calculation mesh before adaptive process. (b) Calculation mesh with new points after adaptive process

$\mathbf{I}^t$ identity vector

$\boldsymbol{\omega}^{*t}$ whose dimension is N_B^t; ω_i^{*t} represents the vorticity at point i on the boundary lines at iteration t

$\boldsymbol{\psi}^{*t}$ whose dimension is N_B^t; ψ_j^{*t} represents the streamfunction at point i on the boundary lines at iteration t—on the boundary lines representing the horizontal or vertical rigid wall ψ_i^{*t} is equal to zero; on the boundary line representing the free surface ψ_i^{*t} is equal to the flow rate Q^*; on the boundary line representing the inflow ψ_i has an assigned value

$\boldsymbol{\omega}'^t$ whose dimension is N_B^t; $\omega_i'^t$ is different from zero only if point i is located on the line representing the inflow

$\mathbf{V}^t$ whose dimension is N^t; V_i^t is the value of the eddy viscosity at point i.

The following topological matrices are defined:

$\mathbf{Q}$ whose dimensions are $N^t \times N^t$; Q_{ij} is different from zero and equal to one only if point-j belongs to the cross having point i as centre

$\mathbf{R}$ whose dimensions are $N^t \times N^t$; R_{ij} is different from zero and assumes the value ± 1 only if point j is the upper or the lower point of the cross having point i as centre

$\mathbf{S}$ whose dimensions are $N^t \times N^t$; S_{ij} is different from zero and assumes the value ± 1 only if point j is the right or left point of the cross having point i as centre

$\mathbf{E}$ whose dimensions are $N_B^t \times N^t$; E_{ij} is different from zero and is equal to one only if point j is not located on the boundary lines but belongs to the cross whose centre is the point i located on the boundary line

$\mathbf{B}$ whose dimensions are $N_B^t \times N_B^t$; B_{ij} is different from zero and equals one only if point j is located on the boundary lines, with the exception of the lines representing the inflow and the free surface

$\mathbf{C}$ whose dimensions are $N^{t+1} \times N^t$; C_{ij} is different from zero and equal to one only if $i=j$

$\mathbf{D}$ whose dimensions are $N^{t+1} \times (N^{t+1} - N^t)$; D_{ij} is different from zero and equal to only if $i - N^t = j$

$\mathbf{U}_i$ i matrix whose dimensions are $N^t \times N^t$; $U_{i_{jk}}$ is different from zero and equal to one only if $i=j=k$.

Once specified that the superscript symbol T defines the operation of vector transposition and that Δt is the time step integration, the calculation iteration to integrate the motion equations is as follows.

(1) Computation of vorticity at the points located within the boundary lines at iteration $t+1$:

$$\omega^{t+1} = \omega^t - \frac{\Delta t}{4}\left(\sum_{i=1}^{N^t}[(\mathbf{U}_i\mathbf{H})\,(\mathbf{U}_i\mathbf{H})^{\mathrm{T}}]\right)^{-1}\left[\left(\sum_{i=1}^{N^t}(\mathbf{R}\,\psi^t-\mathbf{S}\,\mathbf{V}^t)\,(\mathbf{U}_i\mathbf{S}\,\omega^t)^{\mathrm{T}}\right)\boldsymbol{I}\right.$$
$$\left.-\left(\sum_{i=1}^{N^t}(\mathbf{S}\,\psi^t+\mathbf{R}\,\mathbf{V}^t)\,(\mathbf{U}_i\mathbf{R}\,\omega^t)^{\mathrm{T}}\right)\boldsymbol{I}-\left(\sum_{i=1}^{N^t}4[\mathbf{Q}\,\omega^t-4(U_i\,\omega^t)]\,(\mathbf{U}_i\,\mathbf{V}^t)^{\mathrm{T}}\right)\boldsymbol{I}\right]. \tag{25}$$

(2) Computation of streamfunction at iteration $t+1$:

$$\psi^{t+1} = \psi^t + \Delta t\left[\left(\sum_{i=1}^{N^t}[(\mathbf{U}_i\mathbf{H})\,(\mathbf{U}_i\mathbf{H})^{\mathrm{T}}\right)^{-1}(\mathbf{Q}\,\psi^t-4\psi^t)\right]-\Delta t\,\omega^t. \tag{26}$$

(3) Computation of the vorticity at the points located on the boundary lines at iteration $t+1$:

$$\omega^{*t+1} = 2\left(\sum_{i=1}^{N_{\mathrm{B}}^t}(\mathbf{U}_i\mathbf{H})\,(\mathbf{U}_i\mathbf{H})^{\mathrm{T}}\right)^{-1}[(\mathbf{B}\,\mathbf{E}\,\psi^{t+1}-\psi^*)]+(\mathbf{I}-\mathbf{B})\,\mathbf{E}\,\omega^{t+1}+\omega'. \tag{27}$$

(4) Computation of the turbulent kinetic energy and the viscous dissipation at iteration $t+1$ at integration domain internal points; this calculation has been made by finite difference approximation of equations (10) and (11) in the same way as defined in step (1).

(5) Introduction of new symmetrical crosses and new points in the calculation grid. F_{T} is a scalar quantity that regulates the thickening of the mesh; it introduces a new point where the sum of the derivatives of the vorticity is greater than F_{T}. The number of points at iteration $t+1$ is

$$N^{t+1} = N^t + \mathbf{I}^t\left(\sum_{i=1}^{N^t}\mathbf{U}_i[\mathbf{R}\,\omega+\mathbf{S}\,\omega-F_{\mathrm{T}})-|\mathbf{R}\,\omega+\mathbf{S}\,\omega-F_{\mathrm{T}}|]^{\mathrm{T}}\right)^{-1}[(\mathbf{R}\,\omega+\mathbf{S}\,\omega-F_{\mathrm{T}})$$
$$-|\mathbf{R}\,\omega+\mathbf{S}\,\omega-F_{\mathrm{T}}|]. \tag{28}$$

(6) Modification of the vectors and matrices **H**, **R**, **S**, **Q**, **E**, **B**, **C** and **D**.

(7) Computation of the vorticity and the streamfunction at the new points; $\omega_+^{t+\Delta t}$ and $\psi_+^{t+\Delta t}$ are the vorticity and streamfunction vectors that contain the values of those quantities at the new points:

$$\omega_+^{t+1} = \mathbf{C}\,\omega^{t+1}+\mathbf{D}\left\{\frac{1}{4}\left(\sum_{i=1}^{N^{t+1}}\mathbf{U}_i\mathbf{V}\right)^{-1}\left[-\frac{1}{4}\left(\sum_{i=1}^{N^{t+1}}\mathbf{R}\,\psi^{t+1}\,(\mathbf{U}_i\mathbf{S}\,\omega^{t+1})^{\mathrm{T}}\right)\mathbf{I}\right.\right.$$
$$\left.\left.+\frac{1}{4}\left(\sum_{i=1}^{N^{t+1}}\mathbf{S}\,\psi^{t+1}\,(\mathbf{U}_i\mathbf{R}\,\omega^{t+1})^{\mathrm{T}}\right)\mathbf{I}+\mathbf{Q}\,\omega\right]\right\}, \tag{29}$$

$$\psi_+^{t+1} = \mathbf{C}\,\psi^{t+1}+\frac{1}{4}\mathbf{D}\left[\mathbf{Q}\,\psi^{t+1}-\left(\sum_{i=1}^{N^{t+1}}(\mathbf{U}_i\mathbf{H})(\mathbf{U}_i\mathbf{H})^{\mathrm{T}}\right)\omega_+^{t+1}\right]. \tag{30}$$

(8) Computation of the kinetic energy turbulence and the viscous dissipation at the newly introduced points at iteration $t+1$.

APPLICATION

The bidimensional model presented has been used to obtain the velocity and concentration fields in the rectangular sedimentation tank shown in Figure 1.

The tank is 2·00 m high an 20 m long. The flow rate is 0·04 $m^2 s^{-1}$; the values of the characteristic length L_0 and the characteristic velocity U_0 are assumed to be equal to 1·5 m and 0·02 $m s^{-1}$ respectively.

Figure 3 shows the initial computational mesh: the mesh is finer in proximity to the walls and to the outlet an inlet. This thickening of the mesh is needed at the start of the calculation since great accuracy is required in these regions of the domain. In fact, the values for the vorticity in proximity to the wall are approximated in terms of finite difference as a function of the streamfunction; this approximation turns out to be more accurate and more stabilized the finer the mesh is in proximity to the wall.

Figure 4 shows the computational mesh at an intermediate time of calculation, while in Figure 5 the final computational mesh is shown, related to the situation in which the stationary configuration is reached.

From the three previous figures, the self-adaptive process of the mesh as a function of the vorticity gradients and their evolution in time can be observed.

Figure 6 shows the velocity field obtained by calculation: the element which characterizes the whole velocity field is found to be the main eddy immediately downstream from the inlet. The reattachment point is rather far from the inlet and is located at approximately 6·5 tank depths

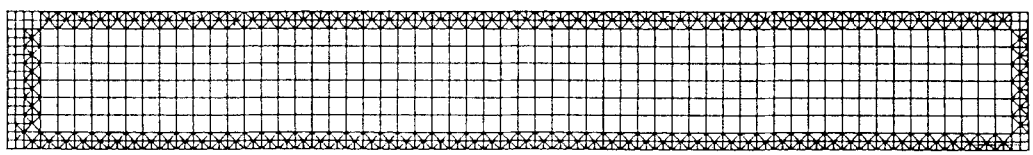

Figure 3. Initial computational mesh

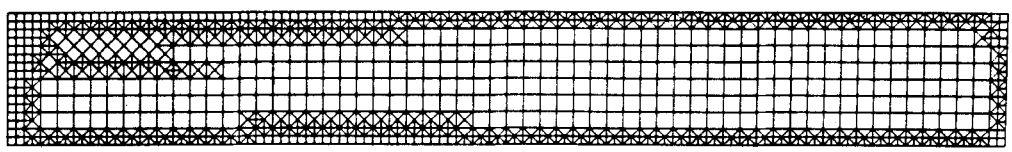

Figure 4. Computational mesh at an intermediate time of calculation

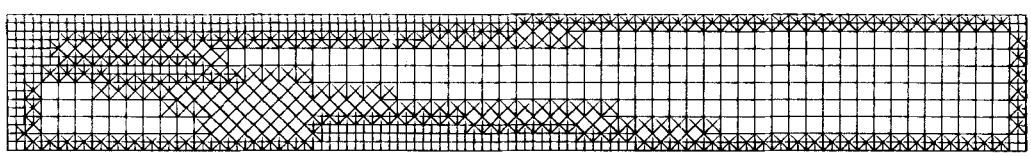

Figure 5. Final computational mesh

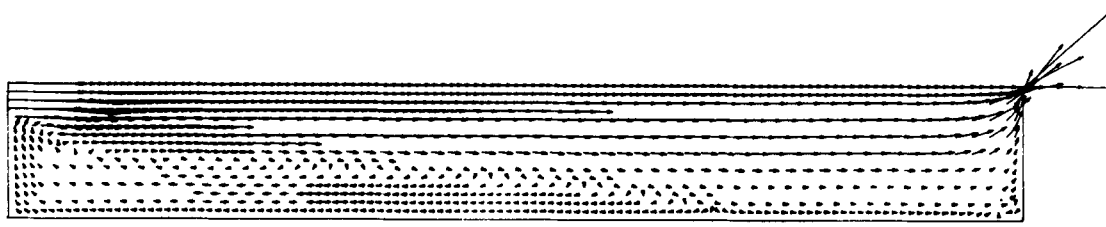

Figure 6. Velocity field obtained by calculation

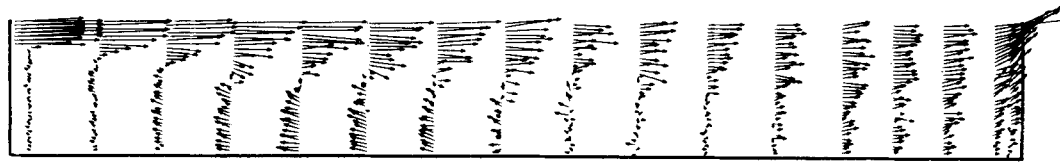

Figure 7(a). Velocity field obtained by measurement with LDA

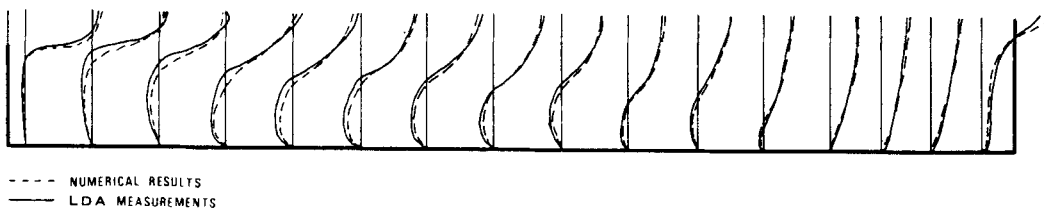

Figure 7(b). Comparison between numerical results and experimental data (velocity profiles)

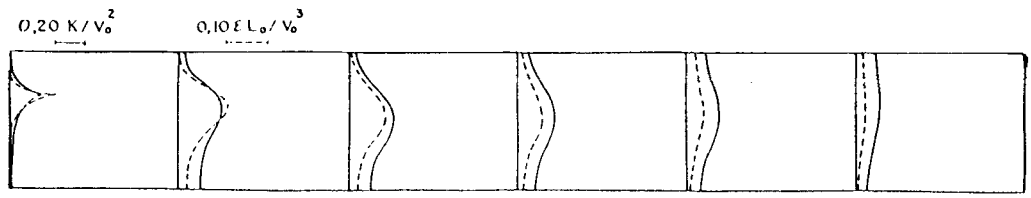

Figure 8. Turbulent kinetic energy andd viscous dissipation

from the inlet. The considerable size of this eddy confirms the importance that the recirculations in the vertical plane have in the analysis of the performance of sedimentation tanks. Experimental data obtained by laser Doppler anemometry in physical tank models with geometry similar to the one shown in Figure 1 are presented in Figure 7(a). Figure 7(b) shows a comparsion between horizontal velocity components obtained by experimental measurements and by the numerical model. By means of this comparison it is possible to point out that the numerical data appear to be in a good agreement with the experimental data. In fact, in the numerical computation the distance between the 'reattachment point' of the main eddy and the inlet is close to the measured distance. Some differences between velocity contours are recognizable near the inlet: the points where the horizontal velocity is equal to zero are in different zones; in the numerical results these points are closer to the bottom of the tank. The aforesaid disagreement is related to the finite

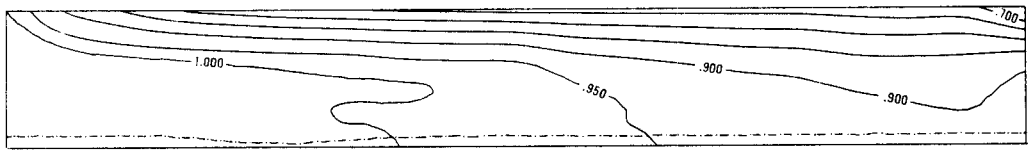

Figure 9. Concentration field and bed thickness; particle diameter 75 μm

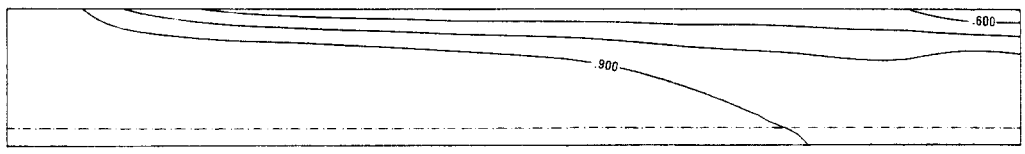

Figure 10. Concentration field and bed thickness; particle diameter 85 μm

difference approximation introduced in the vorticity boundary condition for point B (Figure 1); further thickening of the mesh in the proximity of the inlet can allow an improvement of the numerical outcome.

Figure 8 gives the profiles of turbulent kinetic energy and viscous dissipation. We can see the large values of the turbulent kinetic energy in proximity to the corner at the inlet as well as the effects produced by energy transport in the recirculating zone; these results are in good qualitative agreement with the results obtained by Smith.[14]

The concentration field and the settled bed increase have been simulated for 1 h of real time for different particle diameter values and different sedimentation velocity values.

Figure 9 shows the concentration field and the bed thickness (with a deformed scale) obtained with a particle diameter of 75 μm and a sedimentation velocity of 0·031 cm s^{-1}; in Figure 10 the particle diameter is 85 μm and the sedimentation velocity is 0·039 cm s^{-1}; in Figure 11 the diameter is 115 μm and the velocity is 0·072 cm s^{-1}. The particle density is 1·1 g cm^{-3}. A zero value of the concentration is taken as the initial condition.

From Figure 9 it is possible to deduce the effect that the main eddy has on the concentration field; in particular, the maximum concentration curve is deformed by the change in the advective transport sign produced by the same eddy.

It is also important to note the effect that the upward velocity component close to the wall at the outlet produces on the isoconcentration curves.

The removal efficiency E_f is defined by

$$E_f = \frac{c_0 - c_u}{c_0} \times 100, \tag{31}$$

where c_0 is the inlet concentration and c_u is the outlet concentration. In the case of Figure 9 this efficiency is equal to 37% since the sedimentation velocity is low. In the case of Figures 10 and 11 the removal efficiency is increased as the sedimentation velocity is raised.

Figure 12 shows the removal efficiency curve as a function of the sedimentation velocity.

The bed thickness along the bottom line shown in Figure 9 points out that the suspension phenomenon is larger where the values of the veloicty component parallel to the bed are bigger.

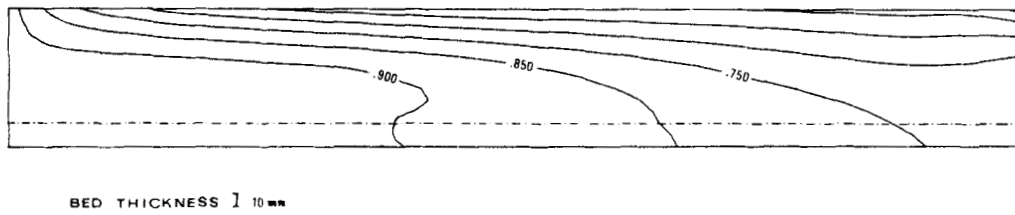

Figure 11. Concentration field and bed thickness; particle diameter 115 μm

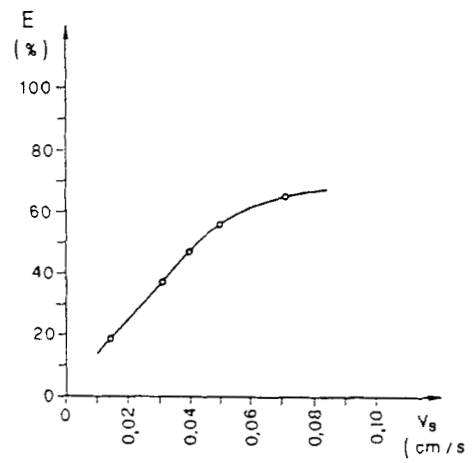

Figure 12. Removal efficiency curve

Figures 9 and 10 give different shapes for the bed thickness; in fact, in this case the suspension phenomenon is less important because the sedimentation velocity is higher.

CONCLUSIONS

The numerical model proposed allows complete simulation of the velocity and concentration fields in primary rectangular sedimentation tanks operating at neutral density condition.

This method, based upon a self-adaptive calculation grid, allows for good simulations in high-gradient regions where calculation instabilities arise. The use of the k–ε model in the simulation of turbulence in sedimentation tanks is imposed by the difficulty in specifying *a priori* the distribution of the eddy viscosity coefficient.

The velocity field obtained by the present calculations shows the existence of a non-uniform recirculating flow pattern within the basin, in good agreement with experimental data obtained with laser Doppler anemometry.

The methodologies used to simulate the suspension particles from the settled bed permit calculation of the removal efficiency of settling tanks without *a priori* specification of the suspension coefficient.

APPENDIX: NOTATION

$\mathbf{B}$	topological matrix of dimensions $N_B^t \times N_B^t$
$\mathbf{C}$	topological matrix of dimensions $N^{t+1} \times N^t$
c	concentration
c_{ar}	reference concentration
c_0	inlet concentration
c_k	suspension coefficient
c_u	outlet concentration
$\mathbf{D}$	topological matrix of dimensions $N^{t+1} \times (N^{t+1} - N^t)$
d	particle diameter
$\mathbf{E}$	topological matrix of dimensions $N_B^t \times N^t$
E_f	removal efficiency
F_T	scalar quantity
$\mathbf{H}$	vector of dimension N^t
$\mathbf{H}^*$	vector of dimension N_B^t
$\mathbf{I}$	identity vector or matrix
N^t	number of points within the boundary lines at iteration t
N_B^t	number of points on boundary lines at iteration t
P	turbulent kinetic energy production
$\mathbf{Q}$	topological matrix of dimensions $N^t \times N^t$
$\mathbf{R}$	topological matrix of dimensions $N^t \times N^t$
$\mathbf{S}$	topological matrix of dimensions $N^t \times N^t$
$\mathbf{T}$	vector transposition exponent
$\mathbf{V}$	vector of dimension N^t; eddy viscosity
k	kinetic energy of turbulence
u	velocity component along x
u_τ	friction velocity
u_r	velocity component parallel to the wall
u_{cr}	critical velocity
$\mathbf{U}_i$	topological matrix
U_r	velocity component parallel to the wall
U_τ	friction velocity
v	velocity component along y
v_s	sedimentation velocity
v_{st}	Stokes' velocity
$\mathbf{v}$	vector of dimension N^t
z	bed thickness, changing in time
ν	kinematic viscosity coefficient
ε	viscous dissipation
ψ	streamfunction
$\boldsymbol{\psi}$	vector of dimension N^t
$\boldsymbol{\psi}^*$	vector of dimension N_B^t
ω	vorticity
$\boldsymbol{\omega}$	vector of dimension N^t
$\boldsymbol{\omega}^*$	vector of dimension N_B^t
$\boldsymbol{\omega}'$	vector of dimension N_B^t
σ_T	Schmidt's number

ν_T eddy viscosity coefficient
χ von Karman's constant

REFERENCES

1. R. R. Hudgins and P. L. Silveston, 'Discuss', *J. Environ. Eng., ASCE*, **110,** 860 (1984).
2. E. Imam and J. A. McCorquodale, 'Simulation of flow in rectangular clarifiers', *J. Environ. Eng., ASCE*, **109,** 713–730 (1983).
3. J. A. McCorquodale, 'Discuss', *J. Environ. Eng., ASCE*, **110,** 861 (1984).
4. D. R. Schamber and B. E. Larock, 'Discuss', *J. Environ. Eng., ASCE*, **110,** 863–864 (1984).
5. M. Di Giacinto, R. Piva and F. Sabetta, 'Two-way coupling effects in dilute gas particle flow', *14th Biennial Fluid Dynamics Symp.* Poland, 1979.
6. D. R. Schamber and B. E. Larock, 'Numerical analysis of flow in sedimentation basins', *J. Hydraul. Div., ASCE*, **107,** 575–591 (1981).
7. W. Rodi, *Turbulence Models and their Application in Hydraulics*, International Association for Hydraulics Research, 1980.
8. S. M. Abdel-Gawad and J. A. McCorquodale, 'Strip integral method applied to Settling Tanks', *J. Hydraul. Div., ASCE*, **110,** 1–17 (1984).
9. O. Hinze, *Turbulence*, McGraw-Hill, New York, 1975, pp. 280–282.
10. B. E. Launder and D. B. Spalding, 'The numerical computation of turbulent flows', *Comput. Methods Appl. Mech. Eng.*, **3,** 269–289 (1974).
11. A. Armanini and G. Di Silvio, 'Influence of the stream boundary condition on the erosion–deposition processes in open channels', *International Association for Hydraulics Research, 19th Congr.*, Melbourne, August 1985.
12. L. C. van Rijn, 'Sediment transport, Part II: Suspended load transport', *J. Hydraul. Div., ASCE*, **110,** 1613–1641 (1984).
13. F. Gallerano, 'Campi di velocità in driven-cavity con alti numeri di reynolds', *Internal Communication, Department 37*, University of Rome 'La Sapienza', 1986 (in Italian).
14. R. M. Smith, 'On the finite-element calculation of turbulent flow using the k–ε model, *Int. J. numer. methods fluids*, **4,** 303–319 (1984).
15. F. Cioffi and A. Misiti, 'Misura del campo idrodinamico in sedimentatore primario rettangolare mediante anemometria laser–doppler', *Ingegneria Sanitaria, ANDIS*, **1,** 13–22 (January–February 1988) (in Italian).
16. F. Gallerano, 'Campi di velocità e di concentrazione in sedimentatori rettangolari', *Idrotecnica Review*, **3,** 111–119 (May–June 1986) (in Italian).